RESEARCH ARTICLE SUMMARY

NEURODEVELOPMENT

Spatial centrosome proteome of human neural cells uncovers disease-relevant heterogeneity

Adam C. O'Neill†, Fatma Uzbas†, Giulia Antognolli†, Florencia Merino†, Kalina Draganova, Alex Jäck, Sirui Zhang, Giorgia Pedini, Julia P. Schessner, Kimberly Cramer, Aloys Schepers, Fabian Metzger, Miriam Esgleas, Pawel Smialowski, Renzo Guerrini, Sven Falk, Regina Feederle, Saskia Freytag, Zefeng Wang, Melanie Bahlo, Ralf Jungmann, Claudia Bagni, Georg H. H. Borner, Stephen P. Robertson, Stefanie M. Hauck, Magdalena Götz*

INTRODUCTION: The centrosome is an interaction hub composed of two centrioles surrounded by pericentriolar material that collectively exerts many pancellular functions, such as cell division, cell migration, and cilia formation. The centrosome acts as the main microtubule-organizing center (MTOC) in many cells, including stem and progenitor cells, but loses this activity often during differentiation. Very little is known, however, about the extent of its cell type–specific composition and function. Individual proteins have been found to be specific to the centrosome of, for example, neural stem cell subtypes, but whether these are exceptions or the rule is unknown.

RATIONALE: To assess any potential cell type–specific functions of the centrosome, its composition needs to be further investigated. However, no comprehensive proteome of neural centrosomes exists to date, and hence, the differences in centrosome composition between neural and other cell types are unknown. Likewise, the extent of the changes in this organelle's distinct makeup during the differentiation of neural stem cells to neurons has not been explored. Because centrosome dysfunction is also linked to many neurodevelopmental conditions, information from such analysis could identify yet unknown disease associations.

RESULTS: To map the centrosome proteome of human neural stem cells and neurons, we chose a spatial proteomic approach to identify not only which proteins are present at this organelle but also where they are localized. Specifically, we selected 10 bait proteins known to localize to distinct sites of the centrosome, immunoprecipitated them from induced pluripotent stem cell–derived neural stem cells and neurons, and reproducibly determined their interactome with mass spectrometry. Interrogation of their interacting partners revealed diversity at this organelle, in which around 60% of the centrosome proteins had not yet been detected at the centrosome in other cell types. Furthermore, upon neuronal differentiation, more than half of these proteins become exchanged for new interactions at specific localizations within the centrosome. The neural centrosome proteomes comprise significantly enriched Gene Ontology terms of RNA-interacting proteins that were not observed in other cell types. Overlapping the neural stem cell and neuron centrosome proteomes with gene variants observed in patients with neurodevelopmental conditions of unknown etiology highlights specific and significant enrichment in epilepsy patients for the neuronal and, in periventricular heterotopia (PH), for the neural stem cell centrosome proteome. With respect to PH, we explored the effect of one candidate variant within the ubiquitously expressed gene that encodes the pre-mRNA processing factor 6 (PRPF6). We chose this candidate because several members of the PRPF6 complex were detected at the neural stem cell centrosome and had variants associated with PH. We show that the specific mutation of PRPF6 recapitulates aspects of the disease phenotype with ectopic cell localization in the periventricular region of the developing mouse cortex. Expression of the mutated form of PRPF6 results in misregulated splicing of, among others, the microtubule-associated protein kinase *Brsk2*. Coexpression of the correctly spliced form—but not the misspliced form, which lacks exon 19—with the mutant PRPF6 rescued the aberrant cell accumulation at the ventricle. The localization of *Brsk2* mRNA at the centrosome is consistent with a role for PRPF6 in bringing its splicing targets to the centrosome for local translation and fine tuning of microtubule function at the centrosome for proper migration out of the periventricular region.

CONCLUSION: Centrosome composition differs between cell types, offering a diversity that is important for development and disease. The ubiquitously expressed protein PRPF6 is enriched at the centrosome in neural stem cells but not neurons, which causes, when mutated, a PH-like phenotype. The extensive characterization of centrosome proteins unraveled in this study provides a rich resource with which to explore further disease associations and cell type– and stage-specific functions. ■

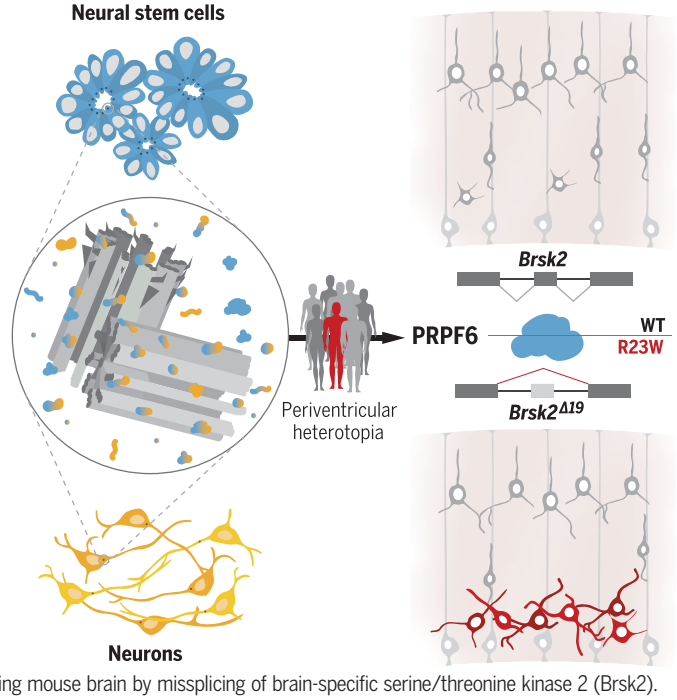

Neural centrosome proteome identifies disease candidates. Spatial proteomics of human neural stem cell and neuronal centrosomes uncovers cell type–specific protein hubs. Overlapping the proteomes with de novo mutations identified in patients with neurodevelopmental diseases revealed cell type–specific disease associations, enabling prioritization of disease variants. Among those, the expression of the PH-associated mutant R23W [in which arginine (R) at position 23 is replaced with tryptophan (W); red] PRPF6 (blue) recapitulated the periventricular cellular misplacement in the developing mouse brain by missplicing of brain-specific serine/threonine kinase 2 (Brsk2).

The list of author affiliations is available in the full article online.
***Corresponding author. Email: magdalena.goetz@helmholtz-muenchen.de**
†These authors contributed equally to this work.
Cite this article as A. C. O'Neill *et al.*, *Science* 376, eabf9088 (2022). DOI: 10.1126/science.abf9088

READ THE FULL ARTICLE AT
https://doi.org/10.1126/science.abf9088

RESEARCH ARTICLE

NEURODEVELOPMENT

Spatial centrosome proteome of human neural cells uncovers disease-relevant heterogeneity

Adam C. O'Neill[1,2]†, Fatma Uzbas[1,2]†, Giulia Antognolli[1,2]†, Florencia Merino[1,2]†, Kalina Draganova[1,2], Alex Jäck[1,2], Sirui Zhang[3,4,5], Giorgia Pedini[6], Julia P. Schessner[7], Kimberly Cramer[7,8], Aloys Schepers[9]‡, Fabian Metzger[10]§, Miriam Esgleas[1,2], Pawel Smialowski[1,2], Renzo Guerrini[11], Sven Falk[1,2], Regina Feederle[9,12], Saskia Freytag[13,14], Zefeng Wang[3,4,5], Melanie Bahlo[13,14], Ralf Jungmann[7,8], Claudia Bagni[6,15], Georg H. H. Borner[7], Stephen P. Robertson[16], Stefanie M. Hauck[10], Magdalena Götz[1,2,12]*

The centrosome provides an intracellular anchor for the cytoskeleton, regulating cell division, cell migration, and cilia formation. We used spatial proteomics to elucidate protein interaction networks at the centrosome of human induced pluripotent stem cell–derived neural stem cells (NSCs) and neurons. Centrosome-associated proteins were largely cell type–specific, with protein hubs involved in RNA dynamics. Analysis of neurodevelopmental disease cohorts identified a significant overrepresentation of NSC centrosome proteins with variants in patients with periventricular heterotopia (PH). Expressing the PH-associated mutant pre-mRNA-processing factor 6 (PRPF6) reproduced the periventricular misplacement in the developing mouse brain, highlighting missplicing of transcripts of a microtubule-associated kinase with centrosomal location as essential for the phenotype. Collectively, cell type–specific centrosome interactomes explain how genetic variants in ubiquitous proteins may convey brain-specific phenotypes.

The centrosome acts as a hub for the cytoskeleton and regulates many processes in development (*1*). It is composed of two centrioles of differing maturity, called the mother and daughter centrioles (*2*). Microtubules are anchored at the more mature mother centriole through its subdistal appendages (*3*). This feature is central to the function of the centrosome as the primary microtubule-organizing center (MTOC) in animal cells (*4*, *5*). Centrosomal MTOC activity changes during development, increasing, for example, in delaminating neural stem cells (NSCs) and decreasing in migrating neurons, a process that is regulated by the newly identified centrosomal protein formerly named AT-hook-containing transcription factor (AKNA) (*6*). Although centrosome proteomes have been cataloged for cancer cells and *Drosophila* (*7*–*10*), the dynamic relationship of AKNA with the centrosome highlights the need to comprehensively investigate the potential heterogeneity of centrosome interactors in brain cells. We identified the centrosome proteome of human NSCs and neurons, showing their cell type–specific relevance to the neurodevelopmental disorder periventricular heterotopia (PH).

Results

Spatial centrosome proteome of NSCs and neurons

To investigate the centrosome proteome of human NSCs and neurons, induced pluripotent stem cells (iPSCs) were differentiated toward a dorsal forebrain identity (Fig. 1A) (*11*). At day 15 of differentiation, almost all cells (96.6%) were PAX6$^+$ NSCs (Fig. 1, B and D, and fig. S1A), whereas neurons reached high purity at around day 40 (Fig. 1, C and D, and fig. S1A) and exhibited known centrosome dynamics, such as NINEIN loss from this organelle (Fig. 1, E to G) (*12*). We therefore chose these time points to probe the centrosome proteomes of NSCs and neurons by using mass spectrometry.

To inform about the spatial distribution of the interactors at the centrosome, we designed an affinity purification strategy that targets 10 different "bait" proteins essential for correct centrosome function, each localizing at different regions within this organelle (Fig. 1H) (*13*). In NSC cultures harvested at day 15 from four biological replicates, 1401 high-confidence interactions comprising 751 proteins were identified, including many centrosomal proteins from curated reference lists and previous studies (*14*–*18*), thus underscoring the robustness of the approach (Fig. 1H; figs. S1, D to F, and S2H; and table S1). We detected 480 proteins that were not allocated to the centrosome in previously studied cell types (Fig. 1I). As expected, the NSC centrosome proteome is enriched for Gene Ontology (GO) terms related to cell division and microtubule organization, among others (Table 1). However, among the highly significant GO terms (*P* values are provided in Table 1) were also mRNA processing, splicing, and metabolism, which were not present in previous centrosome datasets analyzed in the same manner (Table 1 and table S4). Overlapping protein-protein interaction networks of multiple baits can inform on spatial distribution and organellar dynamics (*19*). We therefore clustered the protein interactions for these 10 bait proteins within a force-directed layout by use of Cytoscape. Bait-prey positions within the network are dependent on their common interactions with other bait proteins, as shown in the spatial projection (Fig. 1, L and M). This revealed enrichment of RNA-interacting proteins at specific baits, including the subdistal appendage proteins centrosomal protein of 170 kDa (CEP170) and outer dense fiber of sperm tails 2 (ODF2) (Fig. 1M). Centrosome localization of these RNA-interacting proteins was not dependent on microtubules because they persisted in the centrosome interactome of NSCs after treatment with microtubule-depolymerizing nocodazole (fig. S3 and tables S1 and S3). Thus, the centrosome interactors detected in NSCs may shed light on brain-specific functions at the centrosome.

To ask whether these interactions were brain-specific or NSC-specific, we applied affinity purification of the same 10 bait proteins in neurons, collected at day 40 of iPSC differentiation (Fig. 1, C and D). This revealed 786 proteins enriched at the centrosome in neurons (Fig. 1, H and J, and tables S2 and S3), with about half of the centrosome interactome present only at one stage—59% in neurons and 57% in NSCs (Fig. 1K). Of these, the majority (64 and 57% in NSCs and neurons, respectively) were not present in other centrosome datasets (Fig. 1, I to K). RNA-related

[1]Physiological Genomics, Biomedical Center (BMC), Ludwig-Maximilians-Universitaet (LMU), Großhaderner Straße 9, 82152 Planegg-Martinsried, Germany. [2]Institute of Stem Cell Research, Helmholtz Center Munich, German Research Center for Environmental Health, Großhaderner Straße 9, 82152 Planegg-Martinsried, Germany. [3]CAS Key Laboratory of Computational Biology, Biomedical Big Data Center, Shanghai Institute of Nutrition and Health, Chinese Academy of Sciences, Shanghai 200031, China. [4]University of Chinese Academy of Sciences, Chinese Academy of Sciences, Shanghai 200031, China. [5]CAS Center for Excellence in Molecular Cell Science, Chinese Academy of Sciences, Shanghai 200031, China. [6]Department of Biomedicine and Prevention, University of Rome Tor Vergata, Via Montpellier 1, 00133 Rome, Italy. [7]Max Planck Institute of Biochemistry, Martinsried, Germany. [8]Faculty of Physics and Center for Nanoscience, LMU, Munich, Germany. [9]Monoclonal Antibody Core Facility, Institute for Diabetes and Obesity, Helmholtz Center Munich, German Research Center for Environmental Health, 85764 Neuherberg, Germany. [10]Research Unit Protein Science and Metabolomics and Proteomics Core, Helmholtz Centre Munich, German Research Center for Environmental Health, 85764 Neuherberg, Germany. [11]Neuroscience Department, Children's Hospital Meyer–University of Florence, Florence, Italy. [12]SYNERGY, Excellence Cluster of Systems Neurology, Biomedical Center, LMU, Planegg-Martinsried, Germany. [13]Personalised Oncology Division, The Walter and Eliza Hall Institute of Medical Research, Parkville, VIC 3052, Australia. [14]Department of Medical Biology, University of Melbourne, Melbourne, VIC 3010, Australia. [15]Department of Fundamental Neurosciences, University of Lausanne, Rue du Bugnon 9, 1005 Lausanne, Switzerland. [16]Department of Women's and Children's Health, Dunedin School of Medicine, University of Otago, Dunedin, New Zealand.
†These authors contributed equally to this work. ‡Present address: Institute of Epigenetics and Stem Cells, Helmholtz Zentrum München, Marchioninistrasse 25, 81377 München, Germany. §Deceased.
*Corresponding author. Email: magdalena.goetz@helmholtz-muenchen.de

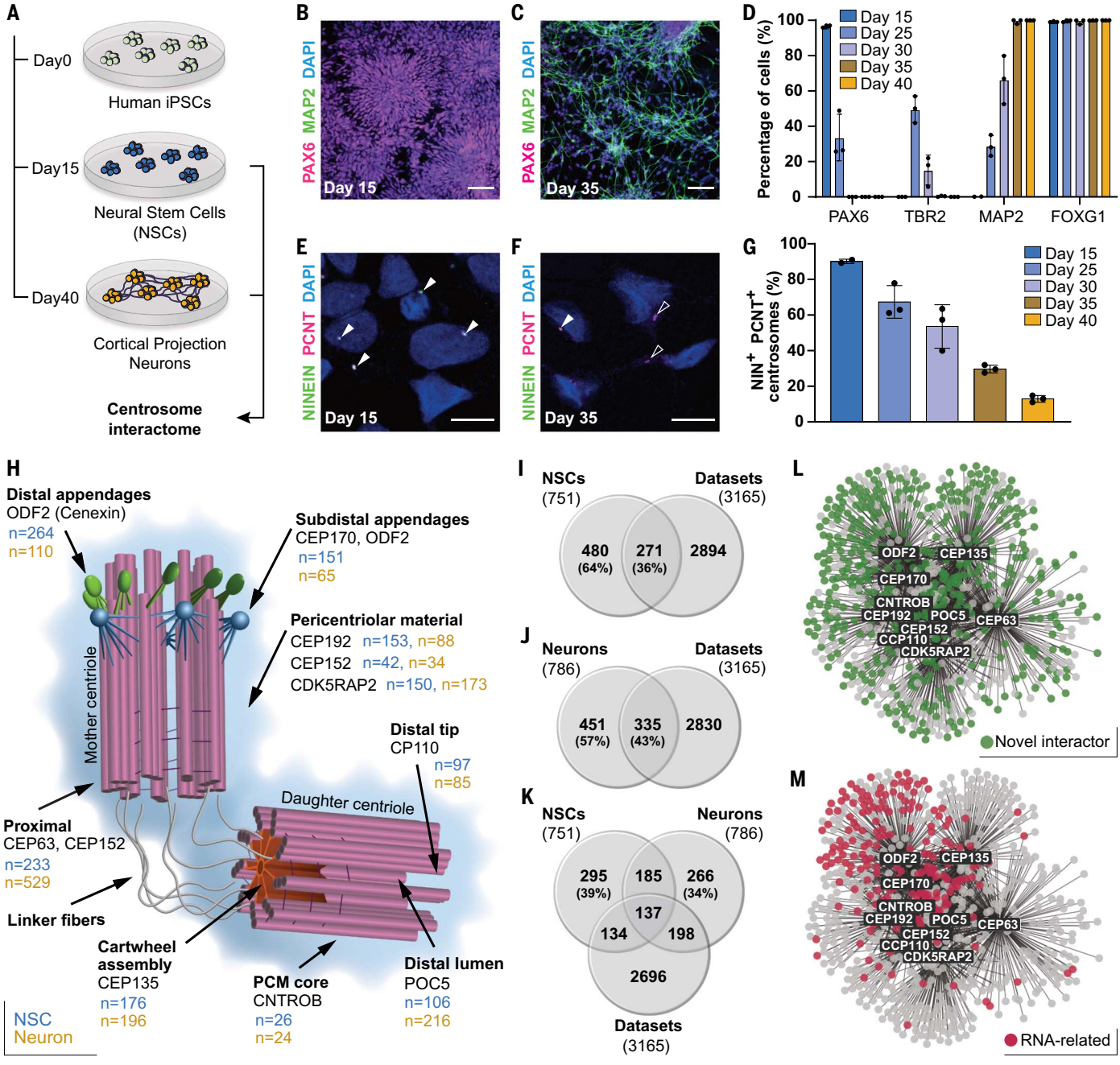

Fig. 1. Spatiotemporal profiling of the neural centrosome interactome. (**A**) Schematic overview of the study design. (**B** to **G**) Immunostainings of human iPSC-derived cells at the stages indicated for antigens indicated on the left, quantified in (D) and (G). Scale bars, (B) and (C) 50 μm; (E) and (F) 10 μm. (**H**) Schematic representation of the mammalian centrosome with the position of the 10 bait proteins indicated, informed by (*13*, *64*), and the number of interactors (*n*) in NSCs (blue) and neurons (yellow). (**I** to **K**) Comparison of the iPSC-derived (I) NSC and (J) neuron centrosome-interactome, with the pooled human centrosome protein list derived from curated databases (*14*, *17*, *18*) and previously published BioID screens (*15*, *16*) and (K) with each other. (**L** and **M**) Force-directed bait-prey interactome of NSCs, with (L) previously unidentified interactors [not found in the datasets in (I) to (K)] (green) and (M) proteins associated with splicing and RNA export-related GO terms (red) highlighted.

functions, such as RNA localization or RNA metabolic processes, remained the top GO terms in both neural proteomes (Table 1 and tables S4 and S8), with RNA splicing selectively enriched in the NSC centrosome proteome (Table 1 and figs. S2, A to F), comprising a complex of pre-mRNA-processing factor 6 (PRPF6), apoptotic chromatin condensation inducer 1 (ACIN1), DEAD-box helicase 23 (DDX23), and protein virilizer homolog (VIRMA/KIAA1429).

Visualization of the spatial centrosome interactomes shows that changes during neuronal differentiation are bait-specific (Fig. 2A; specificity of baits at the centrosome is provided in fig. S4). Most interactors lost during differentiation (significantly enriched at the centrosome in NSCs, but no longer in neurons) are associated with the baits ODF2 and CEP170 at the subdistal appendages and the baits CDK5 regulatory subunit associated protein 2 (CDK5RAP2) and centrosomal protein of

Table 1. GO enrichment for this and previous centrosome databases. Numbers indicate the false discovery rate (FDR) for each term in each dataset indicated (stringency cutoff, 5%). Terms are sorted in ascending order of the FDR difference between NSC and neurons. Complete lists of GO terms are provided in tables S4 and S8.

GO identifier	GO biological process	NSCs	Neurons	Curated databases	BioID screens
GO:0008380	RNA splicing	2.4×10^{-107}*	2.02×10^{-34}		
GO:0016071	mRNA metabolic process	2.4×10^{-107}*	2.19×10^{-66}		
GO:0006405	RNA export from nucleus	4.85×10^{-29}*	2.83×10^{-8}		
GO:0031503	Protein-containing complex localization	6.55×10^{-25}	2.25×10^{-8}	1.39×10^{-16}	3.87×10^{-12}
GO:0006403	RNA localization	2.79×10^{-31}*	5×10^{-17}*		1.21×10^{-6}
GO:0051301	Cell division	2.18×10^{-6}	0.00093	1.39×10^{-38}	7.55×10^{-22}
GO:0071826	Ribonucleoprotein complex subunit organization	1.56×10^{-30}	4.08×10^{-28}		
GO:0000278	Mitotic cell cycle	1.13×10^{-12}	1.18×10^{-14}	2.55×10^{-59}	1.74×10^{-29}
GO:0007018	Microtubule-based movement		0.006	4.69×10^{-58}	7.06×10^{-10}
GO:0007163	Establishment or maintenance of cell polarity		0.0015	1.24×10^{-5}	1.97×10^{-9}
GO:0031023	Microtubule organizing center organization	5.62×10^{-7}	2.16×10^{-10}	9.55×10^{-31}	2.28×10^{-17}
GO:0007098	Centrosome cycle	4.7×10^{-7}	1.28×10^{-10}	6.23×10^{-31}	7.97×10^{-16}
GO:0030705	Cytoskeleton-dependent intracellular transport	0.0078	7.14×10^{-8}	1.25×10^{-26}	9.92×10^{-13}
GO:0030048	Actin filament-based movement		7.33×10^{-6}		
GO:0033119	Negative regulation of RNA splicing		7.07×10^{-6}		
GO:0002252	Immune effector process	0.0022	7.77×10^{-9}		0.0314
GO:0006417	Regulation of translation	2.23×10^{-16}	3.55×10^{-24}		0.0231
GO:0032886	Regulation of microtubule-based process	0.039	5.51×10^{-10}	1.45×10^{-28}	1.52×10^{-12}
GO:0007399	Nervous system development		5.29×10^{-9}	1.96×10^{-12}	1.34×10^{-5}
GO:0000226	Microtubule cytoskeleton organization	4.23×10^{-12}	1.91×10^{-20}	4.03×10^{-94}	6.97×10^{-38}
GO:0070507	Regulation of microtubule cytoskeleton organization	0.0161	1.41×10^{-11}	1.05×10^{-24}	1.89×10^{-16}
GO:0051640	Organelle localization	3.83×10^{-8}	1.14×10^{-19}	2.78×10^{-49}	3.1×10^{-51}
GO:0030036	Actin cytoskeleton organization		4.29×10^{-14}*		6.97×10^{-6}
GO:0030030	Cell projection organization	0.0013	7.58×10^{-19}	2.56×10^{-83}	5.51×10^{-30}
GO:0060271	Cilium assembly	0.00011	5.16×10^{-20}	1.7×10^{-106}	2.71×10^{-35}
GO:0097711	Ciliary basal body-plasma membrane docking	4.86×10^{-11}	6.19×10^{-27}	7.96×10^{-42}	2.94×10^{-39}
GO:0008104	Protein localization	3.16×10^{-10}	4.06×10^{-34}	1.96×10^{-33}	8.16×10^{-52}
GO:0007010	Cytoskeleton organization	3.83×10^{-12}	1.24×10^{-37}	1.37×10^{-60}	5.64×10^{-40}
GO:0006996	Organelle organization	4.42×10^{-14}	9.78×10^{-41}	1.4×10^{-76}	2.32×10^{-61}
GO:0000184	Nuclear-transcribed mRNA catabolic process, nonsense-mediated decay	1.32×10^{-10}	1.36×10^{-42}*		
GO:0006612	Protein targeting to membrane		1.15×10^{-33}*		
GO:0072599	Establishment of protein localization to endoplasmic reticulum		9.06×10^{-40}*		
GO:0006413	Translational initiation	1.83×10^{-10}	2.54×10^{-51}*		

*The notable terms for either cell type.

192 kDa (CEP192) associated with the pericentriolar material (Fig. 2A). This fits with the known loss of centrosome MTOC activity during neuronal differentiation (*6*, *20*), the reduction of CEP170 at the centrosome during cell differentiation, and the role of CEP192 in controlling the balance of centrosomal and noncentrosomal MTOC (*21*–*23*). Centrosome interactors gained in neurons were often associated with centrosomal protein of 63 kDa (CEP63), forming interactions with the actin network and included RNA-interacting proteins enriched at different baits (Fig. 2B and fig. S2) as compared with those in NSCs (Fig. 1M).

Although these dynamic changes imply confidence in the selectivity of the centrosome interactors, we further probed this by comparing with the total cellular proteome (*24*, *25*) of NSCs and neurons differentiated from the same human iPSC line by using the protocol described above. Most of the proteins detected as significantly enriched at the centrosome in neurons, but not NSCs (or vice versa), were not regulated between these cell types within the total proteomes, including proteins further highlighted in this study (fig. S2, I and J). The overall abundance of bait proteins did not change between NSCs and neurons either, with the exception of CEP170 and Centrobin (CNTROB), which are higher in neurons (fig. S2J), but their number of interactors was reduced in neurons or remained the same, respectively (Fig. 1D). Consistent with the lower number of interactors of CEP170 (fig. S1D), its centrosomal association has been shown previously to decrease during differentiation (*23*), and we also found reduced levels at the centrosome by means of immunostaining (fig. S4). Overall, these data corroborate the specificity of the centrosome enrichment in different cell types.

Because the above data suggest neural cell–type specificity of centrosome-interacting proteins with a preponderance to RNA binding and RNA-processing factors in both neural cell types, we next validated sets of those with immunostaining (Fig. 2, C to H, and fig. S5, K to Q) or Western blotting after coimmunoprecipitation with the respective bait proteins (Fig. 2, I to K, and fig. S5, A to J). The centrosome association of the exon-junction proteins (MAGOH

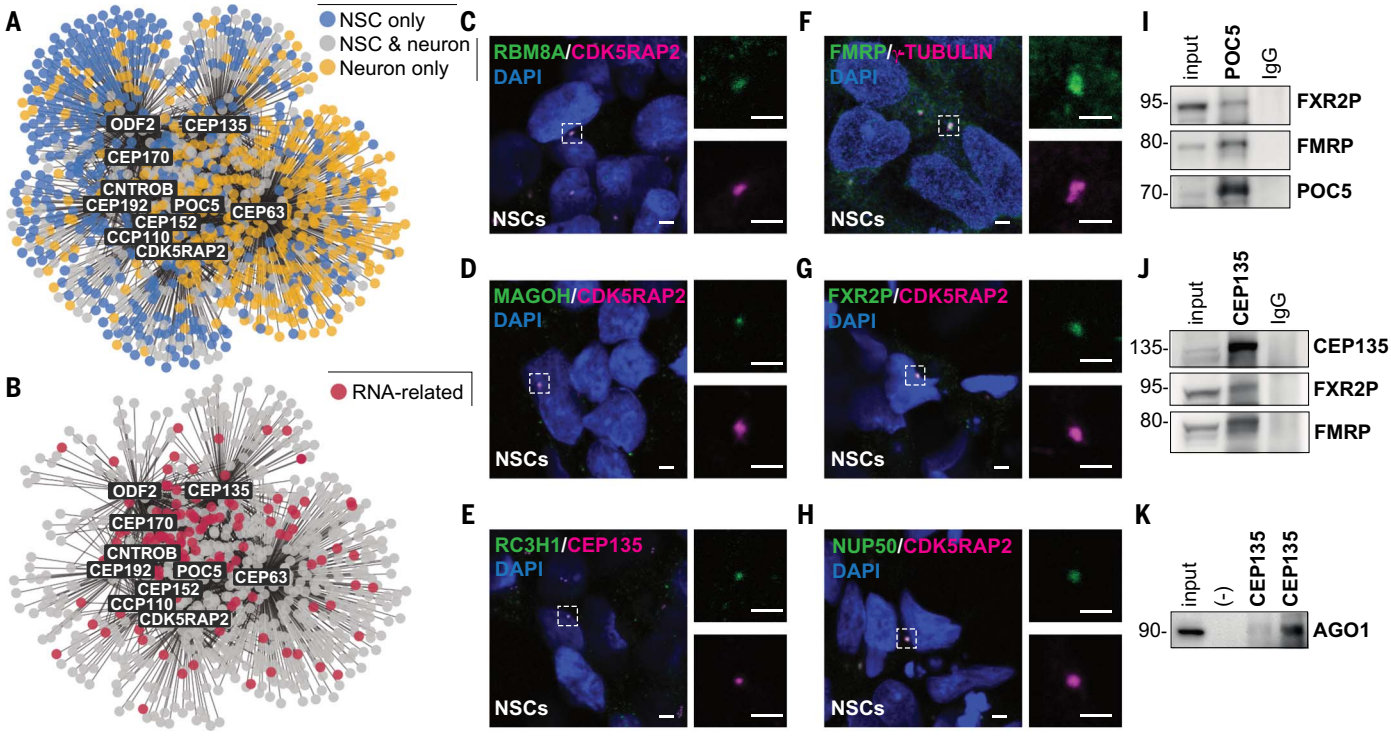

Fig. 2. Cell type–specific RNA-processing proteins at the centrosomes. (**A**) Combined view of the force-directed bait-prey interactomes of the NSC and neuron centrosomes. (**B**) Proteins associated with splicing and RNA export-related GO terms (red) at the neuronal centrosome (NSCs are provided in Fig. 1M). (**C** to **H**) Immunostainings confirming the localization of selected RNA binding proteins at the centrosome in human iPSC-derived NSCs at day 16. White dashed boxes outline colocalization of the proteins indicated in green, with the centrosomal markers in magenta shown to the right in higher magnification. Scale bars, 2.5 μm. (**I** to **K**) Coimmunoprecipitation with bait proteins followed by Western blotting of the indicated preys to validate the liquid chromatography–mass spectrometry (LC-MS)/MS findings. [(I) and (J)] FMRP and FXR2P were pulled down by bait proteins POC5 and CEP135 at day 15, and (K) AGO1 was pulled down by CEP135 at day 35. Further confirmations are available in fig. S5.

Table 2. Overlapping neurodevelopmental disease cohorts and centrosome proteomes. Shown is analysis of the de novo variants per disease gene set per protein list, assessed by means of exact binomial test with Benjamini-Hochberg correction. *P* values were calculated by means of exact binomial test (two-tailed) with Benjamini-Hochberg correction (FDR 0.05). ASD, autism spectrum disorder; PH, periventricular nodular heterotopia; ID, intellectual disability; EE, epileptic encephalopathy; PMG, polymicrogyria.

	Centrosome datasets (*n* = 3165)			NSCs (*n* = 751)			NSCs microtubule-independent (*n* = 625)			Neurons (*n* = 786)		
Disease gene-set*	Expected events	Observed events	*P* value	Expected events	Observed events	*P* value	Expected events	Observed events	*P* value	Expected events	Observed events	*P* value
ASD (*n* = 1918)	285	453	3.26×10^{-23}†	78	135	9.16×10^{-9}†	63	112	6.37×10^{-8}†	76	152	1.16×10^{-14}†
EE (*n* = 356)	53	58	0.5702	14	20	0.1726	12	18	0.1200	14	23	0.0333†
ID (*n* = 192)	29	50	0.0002†	8	13	0.1086	6	9	0.3806	8	18	0.0016†
PH (*n* = 202)	30	34	0.7147	8	16	0.0273†	7	15	0.0104†	8	10	0.4653
PMG (*n* = 86)	13	11	0.7612	3	5	0.4020	3	4	0.3695	3	7	0.1061

*Number of individuals (*n*). †Significant *P* values.

and RBM8A), RNA binding protein Roquin-1 (RC3H1), translation regulators FMRP and FXR2P, RNA processing complex member AGO1, and the nucleoporin NUP50 (Fig. 2, C to K, and fig. S5) [other nucleoporins at the centrosome are available in (*26*)] was confirmed in cultured cells and human fetal cortex samples (fig. S5, I and J). For the latter, we chose gestational week 18 as a later stage of cortex neurogenesis, with many neurons still migrating, which would be most comparable with the stages analyzed in vitro. Thus, three sets of analyses confirm the reliability and specificity of our centrosome interactome analysis.

Significant overlap with specific neurodevelopmental disease cohorts

We next asked whether these neural proteome datasets could be used to inform on genetic variants of unknown etiological relevance in individuals with neurodevelopmental disease. The proteins identified in our centrosome

Table 3. PH-associated de novo variants within individual bait interactomes. Analysis of de novo variants for PH gene-set within the proteome of individual baits in NSCs, assessed by means of exact binomial test with Benjamini-Hochberg correction (FDR 0.05).

NSC, all		NSC, microtubule-independent	
Bait protein	***P* value**	**Bait protein**	***P* value**
CDK5RAP2 (*n* = 150)	0.3318	CDK5RAP2 (*n* = 97)	0.7846
Centrobin (*n* = 26)	0.3808	Centrobin (*n* = 3)	0.0751
CEP63 (*n* = 233)	0.8336	CEP63 (*n* = 176)	0.7785
CEP135 (*n* = 176)	0.3000	CEP135 (*n* = 158)	0.3627
CEP152 (*n* = 42)	1	CEP152 (*n* = 29)	1
CEP170 (*n* = 151)	0.0220*	CEP170 (*n* = 119)	0.0074*
CEP192 (*n* = 153)	0.1634	CEP192 (*n* = 112)	0.0202*
CP110 (*n* = 97)	0.3855	CP110 (*n* = 84)	0.4209
ODF2 (*n* = 264)	0.0107*	ODF2 (*n* = 220)	0.0047*
POC5 (*n* = 106)	0.7534	POC5 (*n* = 86)	0.8335

*Significant *P* values.

proteomes and other publicly available centrosome interactors (*14*–*18*) were overlaid with genes harboring rare de novo variants (DNVs) identified in patients with various neurodevelopmental disorders that still await genetic diagnosis (*27*–*34*). Comparing the overlap of the centrosome proteomes with neurodevelopmental disease cohorts identified several significant overlaps (Table 2 and table S5) that are beyond that expected from natural genetic variation (*35*). First, we observed that autism spectrum disorder (ASD) DNVs showed significant enrichment in all centrosome datasets, supporting pancellular centrosome proteins in disease etiology. Another significant association was observed between DNVs in patients with intellectual disability (ID) and both published centrosome datasets and our neuronal centrosome proteome. Because neurons do not divide, neuronal centrosomes may be particularly relevant for ID owing to their role in cilia formation and function. Conversely, only the NSC centrosome proteome was significantly enriched for proteins encoded by loci with DNVs in the PH cohort databases (Table 2). The failure of some cells to move away from the ventricular lining in PH (*36*) may relate to the centrosomal MTOC activity in NSCs mediating delamination of cells from the ventricle (*6*, *37*). Consistent with this hypothesis, the majority (88%) of the NSC centrosome proteins with DNVs in PH were associated with baits located at microtubule-anchoring centrosome positions (Table 3 and table S5). Almost all (15 of 16) of these proteins driving the PH association were interacting with the centrosome in a microtubule-independent manner (still present in the nocodazole-treated condition) and hence are direct centrosome interactors. Taken together, these data suggest a link between our neural centrosome data and specific neurodevelopmental diseases, with proteins of the NSC and neuronal centrosome proteome enriched in distinct disease cohorts.

PRPF6 variant recapitulates aspects of PH

To determine whether centrosome association of certain proteins indeed helps prioritize DNVs with functional relevance, we investigated the dynamic enrichment of PH DNVs within the centrosome proteomes. Among the microtubule-independent NSC centrosome interactors with PH DNVs, we found four members of an RNA-processing complex: ACIN1, DDX23, KIAA1429, and PRPF6 (Table 2 and tables S1 and S3). Members of this complex were significantly enriched within a set of 40 candidate PH genes whose expression patterns mimic those of known PH loci within human brain transcriptomic data, supporting a relationship to the disease (fig. S6, A and B, and table S6). This prompted us to focus our analysis on the ubiquitously expressed protein PRPF6 because its centrosomal localization along with its associated PH interactors may explain how mutations in this complex induce neurodevelopmental phenotypes. As predicted by the proteome analysis and confirmed with down-regulation, PRPF6 is enriched at the centrosome of NSCs and binds centrosomal and RNA-interacting proteins (Fig. 3, A to F, and fig. S6, E to H). Affinity purification of the RNA binding protein PRPF6 within the human iPSC-derived NSCs pulled down 297 proteins, of which 111 were shared with centrosome proteome (tables S1 and S7), and included a protein complex significantly enriched for genes with DNVs in patients with PH (fig. S6C). This reinforces the plausibility of a contribution of PRPF6 centrosomal localization to the disease phenotype caused by this otherwise ubiquitous protein.

The DNV in *PRPF6* was identified in a male patient born from healthy nonconsanguineous parents, was diagnosed with delayed developmental milestones, and had experienced a single convulsive seizure at 3 years of age. He had severe ID and was nonverbal. Head circumference was at the seventh percentile; brain magnetic resonance imaging (MRI) showed bilateral PH with mildly enlarged Sylvian fissures, and mild frontal lobe and cerebellar hypoplasia. Specifically, the patient has a single, rare (not observed in large genomic sequence datasets) de novo missense variant [c.67C>T, p.Arg23Trp; RefSeq NM_012469.4 (GRCh37)] localized in the Prp1 domain of PRPF6 that directly targets RNA for splicing (*38*). The variant is predicted to be deleterious on the basis of the high Polyphen score and low residual variation intolerance score (*32*).

In the developing mouse brain, *Prpf6* is expressed in both neurons and progenitors (fig. S6D), which is consistent with its overall ubiquitous expression (*39*). Following previous modeling of PH in the developing mouse brain (*40*–*42*), we used in utero electroporation (IUE) to introduce constructs expressing either control [green fluorescent protein (GFP)], wild type ($PRPF6^{WT}$), or $PRPF6^{R23W}$ mutant [in which arginine (R) at position 23 is replaced with tryptophan (W)] into the mouse cortex at embryonic day 13 (E13) (fig. S7, A to C). Analysis at 3 days after electroporation (at E16) showed significantly more GFP^+ cells expressing $PRPF6^{R23W}$ in the periventricular area (Bins 1 and 2, comprising the ventricular and subventricular zones, respectively), with fewer cells reaching the neuronal layers in the cortical plate (Bins 4 and 5) relative to the cells expressing the wild-type form (fig. S7, A to D). Most of the cells expressing $PRPF6^{R23W}$ that were stuck in the subventricular zone succumbed to cell death (fig. S7, E to H), and by 5 days after electroporation at E18, most GFP^+ cells had reached the outer bins in all three conditions (Fig. 3, G to J). However, a significantly increased fraction of cells expressing $PRPF6^{R23W}$ remained located at the periventricular area (Fig. 3, I and J) in a pattern reminiscent of the heterotopia in PH patients. Although this phenotype may not reflect all aspects detected in human patients, the finding of only a minority of cells placed ectopically in periventricular regions, whereas most made it into a normal-appearing grey matter, reflects a common hallmark in PH.

Immunostainings for the NSC marker PAX6, the progenitor marker TBR2, and the neuronal marker TBR1 revealed the mixed composition of the periventricular GFP^+ cells in all three conditions at E18 (Fig. 3, K to S). Most were $PAX6^+$ (Fig. 3, K to M and Q), many were $TBR2^+$ (Fig. 3, K to M and R), and some were $TBR1^+$ (Fig. 3, N to P and S). However, the proportion of $PAX6^+$ NSCs was significantly decreased, whereas neurons were increased in the $PRPF6^{R23W}$ condition (Fig. 3, Q and S). Thus, deficits in delamination and/or migration

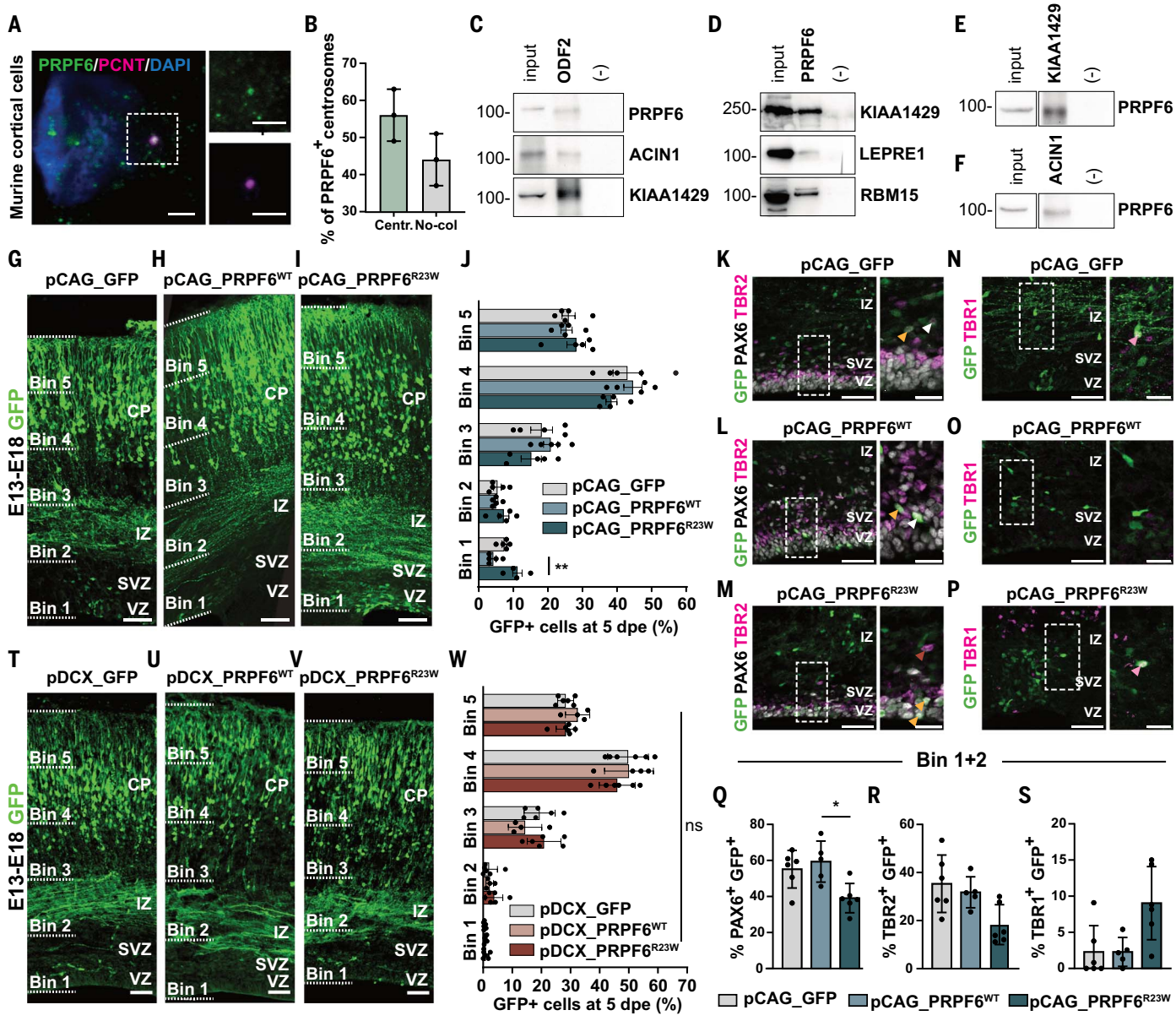

Fig. 3. Centrosomal PRPF6 and its role in PH. (**A**) E14 mouse cortical cells at 3 days in vitro stained as indicated, and (**B**) colocalization quantified (n = 300 in three independent replicates indicated as mean ± SD). Scale bars, 2.5 μm. (**C** to **F**) Coimmunoprecipitation (immunoprecipitation indicated at top) followed by Western blot (antibodies indicated at right) from day 15 iPSC-derived NSCs. (**G** to **I**, **K** to **P**, and **T** to **V**) Coronal sections of E18 mouse cerebral cortices electroporated at E13 with [(G), (K), (N), and (T)] GFP-only control, [(H), (L), (O), and (U)] PRPF6^{WT}, or [(I), (M), (P), and (V)] PRPF6^{R23W} under [(G) to (I) and (K) to (P)] CAG or [(T) to (V)] doublecortin promoter, immunostained as indicated. (**J**) Quantification of (G) to (I) and (**W**) Quantification of (T) to (V). (**Q** and **R**) Quantification of (K) to (M) and (**S**) Quantification of (N) to (P) for GFP$^+$ cells double-positive for the respective markers in Bin 1 and Bin 2; n = embryo; mean ± SD; unpaired two-tailed Kruskal-Wallis test followed with Dunn's multiple comparison; *P < 0.05. Scale bars, (G) to (I) and (T) to (V), 100 μm; (K) to (P), left, 50 μm; (K) to (P), right, 20 μm. Arrows in the periventricular region indicated in (K) to (P) represent double-positive (yellow, white, and pink) or triple-positive (red) cells. VZ, ventricular zone; SVZ, subventricular zone; IZ, intermediate zone; CP, cortical plate; dpe, days post-electroporation.

rather than a failure to differentiate seem to be involved in the periventricular cell positioning. Therefore, we aimed to determine whether the ectopic positioning would also occur when GFP, PRPF6^{WT}, and PRPF6^{R23W} were expressed only in young neurons and differentiating progenitors under the doublecortin regulatory elements (*6*). IUE at E13 followed by analysis at E18 showed no significant difference in the distribution of GFP$^+$ cells for any of the conditions and no ectopic cells in the lower bins (Fig. 3, T to W), suggesting that placement of cells expressing mutant PRPF6 in the periventricular region occurs at earlier stages, before neuronal differentiation. This finding is in agreement with the preferential interaction of the PRPF6 splicing complex with the NSC compared with the neuronal centrosome.

Correctly spliced Brsk2 rescues PRPF6-induced PH

To better understand the etiology of this phenotype, we explored the role of PRPF6 as a

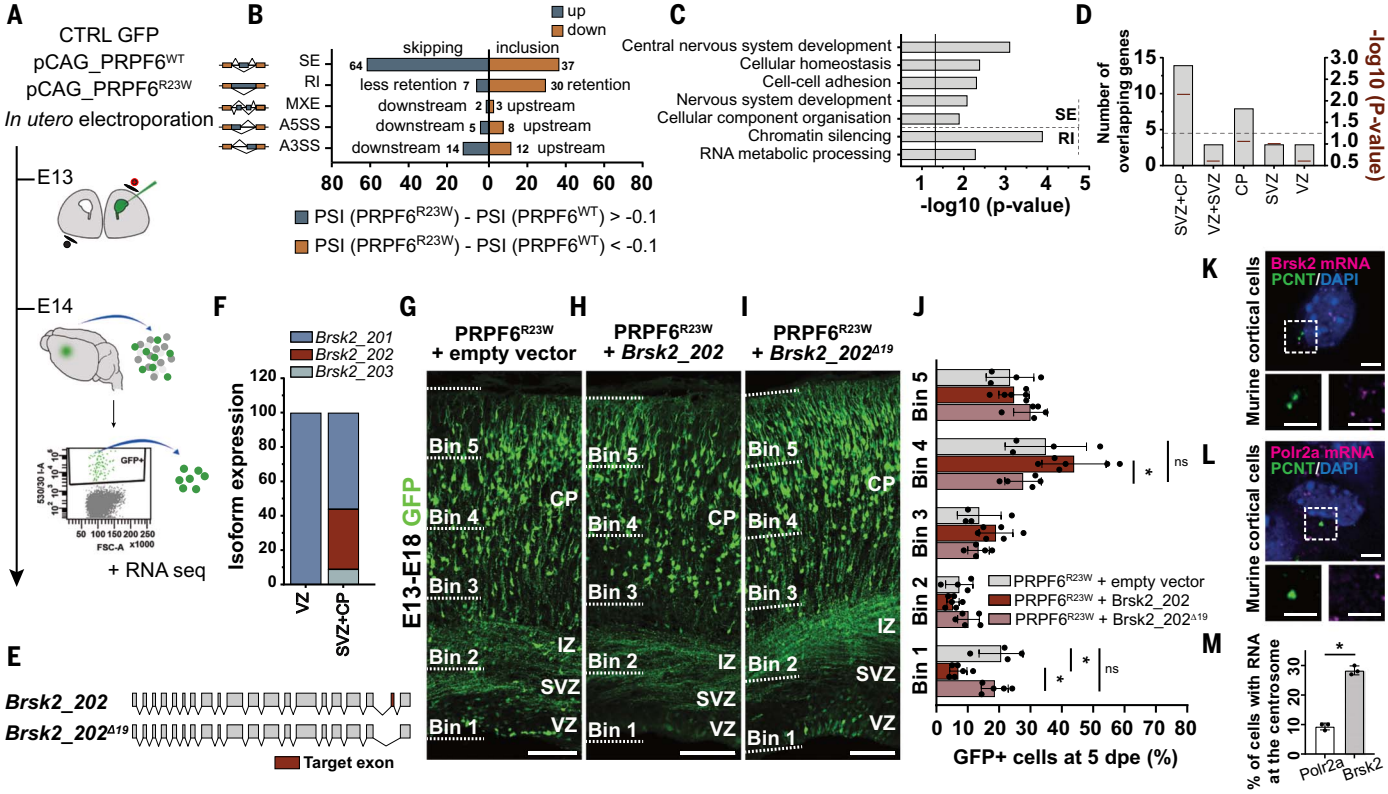

Fig. 4. PRPF6^{R23W} affects splicing in the PH phenotype. (**A**) Schematic representation of the experimental protocol. (**B**) Summary of the splicing changes (indicated as numbers) in cells expressing PRPF6^{R23W} versus PRPF6^{WT}. SE, skipped exon; RI, intron retention; MXE, mutually exclusive exon; A5SS, alternative donor site; A3SS, alternative acceptor site. PSI; percent spliced-in. (**C**) GO analysis (biological processes) of genes with SE or RI in PRPF6^{R23W} versus PRPF6^{WT}-expressing cells. (**D**) Quantification of the number of genes differentially spliced and preferentially expressed in the indicated regions. *P* values with scale are shown on right *y* axis as red bars (Fisher's Exact test, two-tailed, with Benjamini-Hochberg correction). (**E**) Exons (boxes) encoding the *Brsk2_202* transcript isoforms (red; skipped exon in PRPF6^{R23W} cells), introns (lines). (**F**) Regional expression of Brsk2 isoforms (*23*). (**G** to **I**) Coronal sections of E18 mouse cortices coelectroporated at E13 as indicated at top. (**J**) Quantification of (G) to (I) (*n* = embryo; mean ± SD; unpaired two-tailed Kruskal-Wallis test followed with Dunn's multiple comparison; *$P < 0.05$). (**K** and **L**) Single-molecule FISH (magenta) and immunostaining in embryonic mouse cortical cells (3 days in vitro). The white dashed boxes are expanded in the bottom insets. (**M**) Quantification of (K) and (L) (*n* = 300 cells from three independent cultures; mean ± SD; unpaired one-tailed Mann-Whitney test; * $P < 0.05$). Scale bars, (G) to (I) 100 μm; (K) and (L) 2.5 μm. Abbreviations are as in Fig. 3.

regulator of the spliceosome machinery (*38*, *43*). To do so, we performed RNA-sequencing on flow cytometry–purified GFP$^+$ cells at 1 day after electroporation (at E14), before any phenotype could be observed (Fig. 4A and fig. S8, A to D). Only two genes (VCAM1 and a collagen) were differentially expressed between PRPF6^{WT}- and PRPF6^{R23W}-expressing cells (fig. S8E). Using the mixture-of-isoforms (MISO) statistical model, which assigns a "percentage spliced in" (PSI) value to each splicing event (*44*), and choosing the stringent Bayes factor >5, a total of 182 alternative splice events in 166 separate genes were found to be significantly changed between PRPF6^{WT} with PRPF6^{R23W} GFP$^+$ cells (Fig. 4B). These changes encompassed all types of alternative splicing events: 101 alternative cassette exons, 37 intron retention events, five mixed spliced events, as well as 13 and 26 events for alternative donor and acceptor sites, respectively (Fig. 4B). Cells expressing PRPF6^{R23W} showed a bias toward two categories: cassette exon-skipping and intron retention (Fig. 4B), as validated with quantitative reverse transcription polymerase chain reaction (RT-PCR) (fig. S8F). This is consistent with the role of PRPF6 as a core splicing component.

GO term analysis for the genes identified with skipped exons (SEs) or retained introns (RIs) revealed enrichment for categories governing central nervous system development and cell-cell adhesion among SE genes, whereas RI genes were enriched for chromatin silencing and RNA metabolic processing (Fig. 4C). To probe when the genes misspliced upon PRPF6^{R23W} expression may have the greatest effect, we examined their expression using data from the developing mouse cortex (*45*). This showed that genes with skipped exons induced by expression of PRPF6^{R23W} were enriched for loci with significantly greater expression during migration (Fig. 4D). To prioritize possible candidate genes mediating the PH phenotype, we combined the two main enrichment analyses from Fig. 4, C and D, which identified *Ctip2* and *Brsk2*. We selected *Brsk2* because it encodes the SAD-A kinase phosphorylating microtubule-associated proteins (MAPs), regulating microtubule dynamics (*46*, *47*) and neuronal migration in the developing cerebral cortex (*48*).

Of the three *Brsk2* isoforms expressed within the developing mouse brain (*23*), *exon 19* of isoform *Brsk2_202* [RefSeq NM_001009930.3 (GRCh37)] is skipped in the mutant condition (Fig. 4E and fig. S8L). *Brsk2_202* is expressed in cells that leave the ventricle, whereas the isoform *Brsk2_201* [RefSeq NM_001009929.3 (GRCh37)] is expressed in all zones [data are from (*23*)] (Fig. 4F). To test whether *Brsk2_202* plays a role in mediating exit from the ventricular region, PRPF6^{R23W} and *Brsk2_202* were coelectroporated at E13. This resulted in correct cellular distribution within the developing cortex 5 days after electroporation (at

E18) (Fig. 4, G to J), whereas coelectroporation of the misspliced *Brsk2_202* lacking *exon 19* (Brsk2_202$^{\Delta 19}$) did not rescue the PRPF6^{R23W} periventricular phenotype (Fig. 4, I and J). These data implicate the deficiency of this isoform in cells failing to leave the periventricular region and link microtubule-associated processes in migration out of the periventricular region in causing PH phenotypes.

These findings prompted the question of whether NSC centrosome-associated proteins in the highest enrichment category, "splicing," bring their target RNAs to the centrosome. Splicing normally takes place in the nucleus, but the dynamic centrosome association of the PRPF6 complex (which includes ACIN1, DDX23, and KIAA1429 as well as exon junction complex proteins) suggests that RNA processing, transport, and/or translation modulation may be locally regulated by PRPF6. Consistent with this, we detected *Brsk2* RNA by means of single-molecule fluorescence in situ hybridization (FISH) and high-resolution imaging in the proximity of the centrosome in 28.3% of mouse embryonic cortex cells compared with control *Polr2a* RNA (9.3%) (Fig. 4, K to M). RNAs encoding centrosomal proteins have been found at the centrosome in a polysome and translation-related manner (*49*, *50*). These data are consistent with a role of the PRPF6 RNA binding and RNA-processing protein complex at the centrosome, shedding light on how a mutation of this ubiquitous protein causes a phenotype in the developing brain.

Discussion

We used affinity-based proteomics on human iPSC-derived NSCs and neurons targeting 10 core proteins to obtain a spatial portrait of the centrosome proteome. This led to the discovery of hundreds of neural centrosome interactors that were not reported in other centrosome proteomes. Further, this work uncovered dynamic changes of more than half of the centrosome proteome at specific baits during neuronal differentiation. Overlaying this interactome with DNVs of unknown importance from distinct neurodevelopmental disorders identified an enrichment for variants found in individuals with PH within the NSC centrosome proteome. This overlap was not observed for other cell types, including neurons profiled with the same method, which supports centrosome cell-type specificity to be relevant for neurodevelopmental disorders. The centrosome localization of interactors was not restricted to mitosis—as described, for example, for transcriptional regulators localizing to the centrosome or spindle apparatus in mitosis (*51*)—but was rather found in interphase, like AKNA (*6*). Significant enrichment of RNA binding and RNA-processing proteins is prominent in the neural centrosome proteome, and their disease relevance is highlighted by the splicing complex formed by PRPF6 with ACIN1, DDX23, and KIAA1429. Modeling the disease contribution of the PRPF6 mutation detected in a PH patient, our work indicates how ubiquitously expressed genes can contribute to specific disease phenotypes through differential protein network interactions across cell types.

We report the predominance of RNA binding and RNA-modifying proteins, including factors involved in mRNA splicing, RNA transport, and regulation of translation at the neural centrosome proteome, which were not detected in other centrosome proteomes. For example, the three fragile X syndrome proteins—FXR1P, FXR2P, and FMRP—regulate several RNA processes, including translation, transport, and editing (*52*–*57*). Given their link to ASD, exploring their centrosomal function in neural iPSC-derived cells as well as in fetal tissue could elucidate the neurodevelopmental contribution to this condition. Roquin-1 is an RNA binding protein that mediates degradation of its targets and was also detected and validated at the neural centrosome, along with its interactor NUFIP2 (*58*). The recently shown binding of Roquin-1 to *Akna* RNA (*59*) would be consistent with a role in regulating centrosomal MTOC through RNA regulation at the centrosome. Specific mRNA transcripts have been shown to localize at this organelle (such as *PCNT*) (*50*, *60*, *61*), where their local protein translation is detected (*62*). We demonstrated that the RNA for a MAP kinase (SAD-A encoded by *Brsk2*), a splicing target of the PRPF6 complex, also localizes to the centrosome, expanding the concept of function of specific RNAs at this location.

The concept of regulating centrosomal MTOC activity also through local RNAs is further supported by the localization of most of the proteins with PH variants at centrosome baits of the appendages or pericentriolar material (PCM) where microtubules are anchored, including all components of the PRPF6 complex. Centrosomal MTOC activity has been shown to be essential for newly born basal progenitors to migrate away from the brain's ventricle (*6*, *37*). The PRPF6 complex interacts with the centrosome components involved in regulating MTOC, with the de novo PRPF6^{R23W} variant identified in a patient with PH increasing the number of cells remaining in the periventricular region (*6*, *37*). Like AKNA, PRPF6 localizes to the centrosome during interphase and promotes cells' migrating out of the periventricular region. For both proteins, this role occurs before neuronal differentiation because expression under a neuronal promoter failed to elicit a phenotype. The rescue of the heterotopia only with the correctly spliced form of *Brsk2*, but not the one lacking exon 19, further supports the functional relevance of these proteins and their target RNAs at the centrosome for disease. Nascent proteins may exert local functions such as phosphorylation of dynamic microtubule-associated components at the centrosome [reviewed in (*63*)]. Thus, localization of ubiquitously expressed proteins from the PRPF6 complex at the centrosome in NSCs, but not other cells, correlates with their involvement in PH. This not only identifies the microtubule-anchoring region of the centrosome as a hub for PH disease variants but also sheds light on how mutations in genes that encode widely expressed proteins can lead to disorders restricted to the developing brain.

Methods summary

Cell culture

Cortical NSCs and neurons were differentiated from human iPSC lines by using a dual-SMAD inhibition protocol (*11*) with modifications. Cellular identity was confirmed with quantitative RT-PCR and immunostaining.

Coimmunoprecipitation

For proteome analysis, cells were harvested at days 15 (NSCs) or 40 (neurons) of differentiation after treatment with dimethyl sulfoxide (DMSO) or 3.3 μM nocodazole (NSCs only). Cell lysates, each containing 5 mg total protein, were incubated for 1 hour with one of the 10 centrosomal bait antibodies and 2 more hours after adding Protein A and Protein G Dynabeads, with end-to-end rotation at 4°C. Immunoprecipitated lysates were washed with lysis buffer, dissociated by boiling in Laemmli buffer, and stored at −80°C until mass spectometry. Using the same procedure, negative controls were prepared for each of the four replicates parallel to the samples, but bait antibodies were omitted.

Mass spectrometry

Immunoprecipitates were analyzed with mass spectrometry, followed by processing with MaxQuant software (1.6.17.0). Protein enrichment within each immunoprecipitation was calculated with Perseus software (1.6.14.0) by using LFQ intensities through unpaired one-tailed Student's *t* test against the negative controls. GO enrichment of the protein lists was calculated by using the Search Tool for the Retrieval of Interacting Genes/Proteins (STRING) database.

Burden analysis

Disease set enrichment analyses were carried out by using exact binomial test (two-tailed) with Benjamini-Hochberg correction as described previously (*35*), using published de novo variants for ASD, PH, ID, epileptic encephalopathy (EE), and polymicrogyria (PMG) (*27*–*34*).

Immunostaining and single-molecule FISH

Cortical sections and cells were incubated overnight in blocking solution and primary

antibody at 4°C. The day after, they were stained with secondary antibodies diluted in blocking solution and incubated for 1 to 2 hours. For single-molecule FISH combined immunofluorescence, cells were incubated with primary antibody in bovine serum albumin (BSA) and Triton X-100 in 1× phosphate-buffered saline (PBS) and stained with secondary antibodies as described above. After secondary antibody incubation, cells were hybridized with RNA probes overnight at 37°C and thoroughly washed before embedding. Nuclei were visualized by using 4′,6-diamidino-2-phenylindole (DAPI).

Western blot

Immunoprecipitated samples were ran on 6 to 12% SDS gels (depending on the protein size) and then transferred to nitrocellulose membranes. For immunodetection, membranes were first blocked for 1 hour, incubated overnight with primary antibodies, and then washed three times with 1× tris-buffered saline–Polysorbate 20 (TBST) before being incubated with horseradish peroxidase (HRP)–coupled secondary antibodies. The blots were visualized by means of the enhanced chemiluminesence (ECL) method, using a ChemiDoc instrument.

IUE

Endotoxin-free vectors were diluted to 0.5 to 0.7 μg/μl each in 0.9% NaCl and mixed with Fast green, and 1 μl of mix was injected into the ventricles of embryos at E13 in the uterus of anesthetized C57/Bl6 mice and electroporated. Embryonic brains were dissected 1, 3, or 5 days after electroporation and fixed with 4% paraformaldehyde (PFA) in 1× PBS for 2 hours (1 day after electroporation), 4 hours (3 days after electroporation), or 6 hours (5 days after electroporation). For analysis, embryos from at least two females were used, and quantifications were made from two to three coronal sections from four to six embryos. Statistical differences were assessed by means of unpaired Kruskal-Wallis tests followed by Dunn's multiple comparison correction.

REFERENCES AND NOTES

1. M. Wilsch-Bräuninger, W. B. Huttner, Primary cilia and centrosomes in neocortex development. *Front. Neurosci.* **15**, 755867 (2021). doi: 10.3389/fnins.2021.755867; pmid: 34744618
2. P. Gönczy, G. N. Hatzopoulos, Centriole assembly at a glance. *J. Cell Sci.* **132**, jcs228833 (2019). doi: 10.1242/jcs.228833; pmid: 30787112
3. C. Vineethakumari, J. Lüders, Microtubule anchoring: Attaching dynamic polymers to cellular structures. *Front. Cell Dev. Biol.* **10**, 867870 (2022). doi: 10.3389/fcell.2022.867870; pmid: 35309944
4. N. Delgehyr, J. Sillibourne, M. Bornens, Microtubule nucleation and anchoring at the centrosome are independent processes linked by ninein function. *J. Cell Sci.* **118**, 1565–1575 (2005). doi: 10.1242/jcs.02302; pmid: 15784680
5. M. Piel, P. Meyer, A. Khodjakov, C. L. Rieder, M. Bornens, The respective contributions of the mother and daughter centrioles to centrosome activity and behavior in vertebrate cells. *J. Cell Biol.* **149**, 317–330 (2000). doi: 10.1083/jcb.149.2.317; pmid: 10769025
6. G. Camargo Ortega *et al.*, The centrosome protein AKNA regulates neurogenesis via microtubule organization. *Nature* **567**, 113–117 (2019). doi: 10.1038/s41586-019-0962-4; pmid: 30787442
7. J. S. Andersen *et al.*, Proteomic characterization of the human centrosome by protein correlation profiling. *Nature* **426**, 570–574 (2003). doi: 10.1038/nature02166; pmid: 14654843
8. L. Gheiratmand *et al.*, Spatial and proteomic profiling reveals centrosome-independent features of centriolar satellites. *EMBO J.* **38**, e101109 (2019). doi: 10.15252/embj.2018101109; pmid: 31304627
9. H. Müller *et al.*, Proteomic and functional analysis of the mitotic Drosophila centrosome. *EMBO J.* **29**, 3344–3357 (2010). doi: 10.1038/emboj.2010.210; pmid: 20818332
10. G. Sauer *et al.*, Proteome analysis of the human mitotic spindle. *Mol. Cell. Proteomics* **4**, 35–43 (2005). doi: 10.1074/mcp.M400158-MCP200; pmid: 15561729
11. Y. Shi, P. Kirwan, F. J. Livesey, Directed differentiation of human pluripotent stem cells to cerebral cortex neurons and neural networks. *Nat. Protoc.* **7**, 1836–1846 (2012). doi: 10.1038/nprot.2012.116; pmid: 22976355
12. D. K. Moss *et al.*, Ninein is released from the centrosome and moves bi-directionally along microtubules. *J. Cell Sci.* **120**, 3064–3074 (2007). doi: 10.1242/jcs.010322; pmid: 17698918
13. G. A. Pihan, Centrosome dysfunction contributes to chromosome instability, chromoanagenesis, and genome reprograming in cancer. *Front. Oncol.* **3**, 277 (2013). doi: 10.3389/fonc.2013.00277; pmid: 24282781
14. J. M. C. Alves-Cruzeiro, R. Nogales-Cadenas, A. D. Pascual-Montano, CentrosomeDB: A new generation of the centrosomal proteins database for *Human* and *Drosophila melanogaster*. *Nucleic Acids Res.* **42**, D430–D436 (2014). doi: 10.1093/nar/gkt1126; pmid: 24270791
15. E. N. Firat-Karalar, N. Rauniyar, J. R. Yates3rd, T. Stearns, Proximity interactions among centrosome components identify regulators of centriole duplication. *Curr. Biol.* **24**, 664–670 (2014). doi: 10.1016/j.cub.2014.01.067; pmid: 24613305
16. G. D. Gupta *et al.*, A dynamic protein interaction landscape of the human centrosome-cilium interface. *Cell* **163**, 1484–1499 (2015). doi: 10.1016/j.cell.2015.10.065; pmid: 26638075
17. E. Sjöstedt *et al.*, An atlas of the protein-coding genes in the human, pig, and mouse brain. *Science* **367**, eaay5947 (2020). doi: 10.1126/science.aay5947; pmid: 32139519
18. T. J. van Dam, G. Wheway, G. G. Slaats, M. A. Huynen, R. H. Giles; SYSCILIA Study Group, The SYSCILIA gold standard (SCGSv1) of known ciliary components and its applications within a systems biology consortium. *Cilia* **2**, 7 (2013). doi: 10.1186/2046-2530-2-7; pmid: 23725226
19. E. Lundberg, G. H. H. Borner, Spatial proteomics: A powerful discovery tool for cell biology. *Nat. Rev. Mol. Cell Biol.* **20**, 285–302 (2019). doi: 10.1038/s41580-018-0094-y; pmid: 30659282
20. M. Stiess *et al.*, Axon extension occurs independently of centrosomal microtubule nucleation. *Science* **327**, 704–707 (2010). doi: 10.1126/science.1182179; pmid: 20056854
21. M. P. Gavilan *et al.*, The dual role of the centrosome in organizing the microtubule network in interphase. *EMBO Rep.* **19**, e45942 (2018). doi: 10.15252/embr.201845942; pmid: 30224411
22. B. P. O'Rourke *et al.*, Cep192 controls the balance of centrosome and non-centrosomal microtubules during interphase. *PLOS ONE* **9**, e101001 (2014). doi: 10.1371/journal.pone.0101001; pmid: 24971877
23. X. Zhang *et al.*, Cell-type-specific alternative splicing governs cell fate in the developing cerebral cortex. *Cell* **166**, 1147–1162.e15 (2016). doi: 10.1016/j.cell.2016.07.025; pmid: 27565344
24. D. N. Itzhak, S. Tyanova, J. Cox, G. H. Borner, Global, quantitative and dynamic mapping of protein subcellular localization. *eLife* **5**, e16950 (2016). doi: 10.7554/eLife.16950; pmid: 27278775
25. D. N. Itzhak *et al.*, A mass spectrometry-based approach for mapping protein subcellular localization reveals the spatial proteome of mouse primary neurons. *Cell Rep.* **20**, 2706–2718 (2017). doi: 10.1016/j.celrep.2017.08.063; pmid: 28903049
26. R. W. Wong, New activities of the nuclear pore complexes. *Cells* **10**, 2123 (2021). doi: 10.3390/cells10082123; pmid: 34440892
27. J. de Ligt *et al.*, Diagnostic exome sequencing in persons with severe intellectual disability. *N. Engl. J. Med.* **367**, 1921–1929 (2012). doi: 10.1056/NEJMoa1206524; pmid: 23033978
28. A. S. Allen *et al.*, De novo mutations in epileptic encephalopathies. *Nature* **501**, 217–221 (2013). doi: 10.1038/nature12439; pmid: 23934111
29. A. S. Allen *et al.*, Diverse genetic causes of polymicrogyria with epilepsy. *Epilepsia* **62**, 973–983 (2021). doi: 10.1111/epi.16854; pmid: 33818783
30. M. Fromer *et al.*, De novo mutations in schizophrenia implicate synaptic networks. *Nature* **506**, 179–184 (2014). doi: 10.1038/nature12929; pmid: 24463507
31. F. F. Hamdan *et al.*, De novo mutations in moderate or severe intellectual disability. *PLOS Genet.* **10**, e1004772 (2014). doi: 10.1371/journal.pgen.1004772; pmid: 25356899
32. E. L. Heinzen *et al.*, De novo and inherited private variants in MAP1B in periventricular nodular heterotopia. *PLOS Genet.* **14**, e1007281 (2018). doi: 10.1371/journal.pgen.1007281; pmid: 29738522
33. E. T. Lim *et al.*, Rates, distribution and implications of postzygotic mosaic mutations in autism spectrum disorder. *Nat. Neurosci.* **20**, 1217–1224 (2017). doi: 10.1038/nn.4598; pmid: 28714951
34. A. Rauch *et al.*, Range of genetic mutations associated with severe non-syndromic sporadic intellectual disability: An exome sequencing study. *Lancet* **380**, 1674–1682 (2012). doi: 10.1016/S0140-6736(12)61480-9; pmid: 23020937
35. K. E. Samocha *et al.*, A framework for the interpretation of de novo mutation in human disease. *Nat. Genet.* **46**, 944–950 (2014). doi: 10.1038/ng.3050; pmid: 25086666
36. E. Parrini *et al.*, Periventricular heterotopia: Phenotypic heterogeneity and correlation with Filamin A mutations. *Brain* **129**, 1892–1906 (2006). doi: 10.1093/brain/awl125; pmid: 16684786
37. I. Kasioulis, R. M. Das, K. G. Storey, Inter-dependent apical microtubule and actin dynamics orchestrate centrosome retention and neuronal delamination. *eLife* **6**, e26215 (2017). doi: 10.7554/eLife.26215; pmid: 29058679
38. M. Lützelberger *et al.*, The N-terminus of Prp1 (Prp6/U5-102 K) is essential for spliceosome activation in vivo. *Nucleic Acids Res.* **38**, 1610–1622 (2010). doi: 10.1093/nar/gkp1155; pmid: 20007600
39. D. J. Di Bella *et al.*, Molecular logic of cellular diversification in the mouse cerebral cortex. *Nature* **595**, 554–559 (2021). doi: 10.1038/s41586-021-03670-5; pmid: 34163074
40. L. Broix *et al.*, Mutations in the HECT domain of NEDD4L lead to AKT-mTOR pathway deregulation and cause periventricular nodular heterotopia. *Nat. Genet.* **48**, 1349–1358 (2016). doi: 10.1038/ng.3676; pmid: 27694961
41. S. Cappello *et al.*, Mutations in genes encoding the cadherin receptor-ligand pair DCHS1 and FAT4 disrupt cerebral cortical development. *Nat. Genet.* **45**, 1300–1308 (2013). doi: 10.1038/ng.2765; pmid: 24056717
42. A. Carabalona *et al.*, A glial origin for periventricular nodular heterotopia caused by impaired expression of Filamin-A. *Hum. Mol. Genet.* **21**, 1004–1017 (2012). doi: 10.1093/hmg/ddr531; pmid: 22076441
43. G. Tanackovic *et al.*, A missense mutation in PRPF6 causes impairment of pre-mRNA splicing and autosomal-dominant retinitis pigmentosa. *Am. J. Hum. Genet.* **88**, 643–649 (2011). doi: 10.1016/j.ajhg.2011.04.008; pmid: 21549338
44. Y. Katz, E. T. Wang, E. M. Airoldi, C. B. Burge, Analysis and design of RNA sequencing experiments for identifying isoform regulation. *Nat. Methods* **7**, 1009–1015 (2010). doi: 10.1038/nmeth.1528; pmid: 21057496
45. S. A. Fietz *et al.*, Transcriptomes of germinal zones of human and mouse fetal neocortex suggest a role of extracellular matrix in progenitor self-renewal. *Proc. Natl. Acad. Sci. U.S.A.* **109**, 11836–11841 (2012). doi: 10.1073/pnas.1209647109; pmid: 22753484
46. A. P. Barnes *et al.*, LKB1 and SAD kinases define a pathway required for the polarization of cortical neurons. *Cell* **129**, 549–563 (2007). doi: 10.1016/j.cell.2007.03.025; pmid: 17482548
47. M. Kishi, Y. A. Pan, J. G. Crump, J. R. Sanes, Mammalian SAD kinases are required for neuronal polarization. *Science* **307**, 929–932 (2005). doi: 10.1126/science.1107403; pmid: 15705853

48. K. Nakanishi *et al*., Isozyme-specific role of SAD-A in neuronal migration during development of cerebral cortex. *Cereb. Cortex* **29**, 3738–3751 (2019). doi: 10.1093/cercor/bhy253; pmid: 30307479
49. P. V. Ryder, J. Fang, D. A. Lerit, *centrocortin* RNA localization to centrosomes is regulated by FMRP and facilitates error-free mitosis. *J. Cell Biol.* **219**, e202004101 (2020). doi: 10.1083/jcb.202004101; pmid: 33196763
50. G. Sepulveda *et al*., Co-translational protein targeting facilitates centrosomal recruitment of PCNT during centrosome maturation in vertebrates. *eLife* **7**, e34959 (2018). doi: 10.7554/eLife.34959; pmid: 29708497
51. M. P. Somma *et al*., Moonlighting in mitosis: Analysis of the mitotic functions of transcription and splicing factors. *Cells* **9**, 1554 (2020). doi: 10.3390/cells9061554; pmid: 32604778
52. C. Bagni, R. S. Zukin, A synaptic perspective of fragile X syndrome and autism spectrum disorders. *Neuron* **101**, 1070–1088 (2019). doi: 10.1016/j.neuron.2019.02.041; pmid: 30897358
53. D. Cook *et al*., FXR1P limits long-term memory, long-lasting synaptic potentiation, and de novo GluA2 translation. *Cell Rep.* **9**, 1402–1416 (2014). doi: 10.1016/j.celrep.2014.10.028; pmid: 25456134
54. J. K. Davis, K. Broadie, Multifarious functions of the fragile X mental retardation protein. *Trends Genet.* **33**, 703–714 (2017). doi: 10.1016/j.tig.2017.07.008; pmid: 28826631
55. E. Fernández *et al*., FXR2P exerts a positive translational control and is required for the activity-dependent increase of PSD95 expression. *J. Neurosci.* **35**, 9402–9408 (2015). doi: 10.1523/JNEUROSCI.4800-14.2015; pmid: 26109663
56. L.-J. Pilaz, A. L. Lennox, J. P. Rouanet, D. L. Silver, Dynamic mRNA transport and local translation in radial glial progenitors of the developing brain. *Curr. Biol.* **26**, 3383–3392 (2016). doi: 10.1016/j.cub.2016.10.040; pmid: 27916527
57. L.-J. Pilaz, D. L. Silver, Moving messages in the developing brain-emerging roles for mRNA transport and local translation in neural stem cells. *FEBS Lett.* **591**, 1526–1539 (2017). doi: 10.1002/1873-3468.12626; pmid: 28304078
58. G. Behrens, V. Heissmeyer, Cooperation of RNA-binding proteins—A focus on roquin function in T cells. *Front. Immunol.* **13**, 839762 (2022). doi: 10.3389/fimmu.2022.839762; pmid: 35251035
59. K. P. Hoefig *et al*., Defining the RBPome of primary T helper cells to elucidate higher-order Roquin-mediated mRNA regulation. *Nat. Commun.* **12**, 5208 (2021). doi: 10.1038/s41467-021-25345-5; pmid: 34471108
60. S. Hassine *et al*., Staufen1 localizes to the mitotic spindle and controls the localization of RNA populations to the spindle. *J. Cell Sci.* **133**, jcs247155 (2020). doi: 10.1242/jcs.247155; pmid: 32576666
61. A. Safieddine *et al*., A choreography of centrosomal mRNAs reveals a conserved localization mechanism involving active polysome transport. *Nat. Commun.* **12**, 1352 (2021). doi: 10.1038/s41467-021-21585-7; pmid: 33649340
62. D. Iaconis *et al*., The centrosomal OFD1 protein interacts with the translation machinery and regulates the synthesis of specific targets. *Sci. Rep.* **7**, 1224 (2017). doi: 10.1038/s41598-017-01156-x; pmid: 28450740
63. M. W. Breuss, I. Leca, T. Gstrein, A. H. Hansen, D. A. Keays, Tubulins and brain development—The origins of functional specification. *Mol. Cell. Neurosci.* **84**, 58–67 (2017). doi: 10.1016/j.mcn.2017.03.002; pmid: 28347630
64. R. Uzbekov, I. Alieva, Who are you, subdistal appendages of centriole? *Open Biol.* **8**, 180062 (2018). doi: 10.1098/rsob.180062; pmid: 30045886

ACKNOWLEDGMENTS

We thank V. Heissmeyer for Roquin-1 and NUFIP2 antibodies, M. Kiebler for Stau2 antibodies, I. Solovei for Lamin-A antibodies, and M.-E. Torres-Padilla for CRABP2 antibodies; D. L. Silver for suggestions on exon-junction complex proteins; M. Drukker and E. Rusha (HMGU) for the iPSC lines; and M. Bürkle and I. Mühlhahn for their excellent technical help with Western Blotting and cloning, respectively. We are particularly grateful to G. Camargo Ortega and T. Mikeladze-Dvali for providing great centrosome expertise, to G. Camargo Ortega for excellent comments on the manuscript, and to M. Puglisi for help with the graphical abstract. **Funding:** A.C.O. was supported by a Philip Wrightson Postdoctoral Fellowship from the Neurological Foundation of New Zealand. Funding for this work was provided from the ERC (advanced grant NeuroCentro, 885382 to M.G.), the EU (NSC-Reconstruct, 874758, to M.G.), the German Research Foundation [Go 640 12/1, 14/2; Synergy (EXC 2145/ID 390857198), SFB870 to M.G.], and Curekids and the Health Research Council of NZ (to S.P.R.). R.G. was supported by Tuscany Region Call for Health 2018 (grant DECODE-EE), Z.W. was supported by NSFC (grant 31730110), and M.B. was supported by an Australian National Health and Medical Research Council (NHMRC) Fellowship (110297). Funding to C.B. was from PRIN2017 201789LFKB, Telethon GGP20137, and SNSF 310030-182651. This work was also supported by the NHMRC Independent Research Institute Infrastructure Support Scheme (IRIISS to M.B.). J.P.S. and G.H.H.B. were supported by the Max Planck Society for the Advancement of Science, and we thank M. Mann for his continued support. The human embryonic and fetal material was provided by the Human Developmental Biology Resource (https://www.hdbr.org). **Author contributions:** M.G. conceived and designed the project together with A.C.O.; A.C.O. and F.U. performed the NSC and neuron centrosome bait immunoprecipitations, respectively, and F.U. analyzed mass spectrometry data. F.Met. and S.M.H. performed mass spectrometry and informed on proteomics. J.P.S. performed mass spectrometry to determine the overall proteomes of neurons and NSCs; J.P.S. and G.H.H.B. jointly performed the corresponding data analyses. G.A. assessed PRPF6 function in vitro and centrosomal localization across cell-types; K.C. and G.A. performed FISH experiments with guidance by R.J.; F.U., K.D., and G.A. validated centrosome interactors, supervised by M.G., and G.P. by C.B., and K.D. validated PRPF6 interactors and aided in fluorescence-activated cell sorting (FACS) analysis with A.C.O; A.C.O and F.Mer. performed all in vivo experiments, which were also analyzed by A.J.; A.J. analyzed NINEIN dynamics in vitro; A.C.O. and S.Fr. performed analysis on human brain transcriptomic data, with supervision from M.B.; A.S. and R.F. generated monoclonal PRPF6 and NUP50 antibodies; R.G. and S.P.R. contributed clinical phenotyping; and S.P.R. contributed whole-exome sequencing data. M.E. produced PRPF6 constructs; S.Z. and Z.W. performed splicing analysis; P.S. analyzed *Brsk2* isoform expression dynamics; A.C.O. and M.G. wrote the manuscript, and all authors contributed corrections and comments. **Competing interests:** The authors declare no competing interests. **Data and materials availability:** Raw and processed mass spectrometry proteomics data have been deposited to the ProteomeXchange Consortium through the Proteomics Identification Database (PRIDE; https://www.ebi.ac.uk/pride) with the accession number: PXD031936 (https://doi.org/10.6019/PXD031936). The RNA-sequencing data discussed in this manuscript is deposited in NCBI's Gene Expression Omnibus (NCBI-GEO) and is accessible under the Series: GSE201954 (https://www.ncbi.nlm.nih.gov/geo/query/acc.cgi?acc=GSE201954). All other data are in the main paper or supplementary materials.

SUPPLEMENTARY MATERIALS

science.org/doi/10.1126/science.abf9088
Materials and Methods
Figs. S1 to S8
References (*65*–*85*)
Tables S1 to S8
MDAR Reproducibility Checklist

View/request a protocol for this paper from *Bio-protocol*.

Submitted 27 November 2020; resubmitted 31 December 2021
Accepted 5 May 2022
10.1126/science.abf9088